

Dirac-semimetal phase diagram of two-dimensional black phosphorus

Hyeonjin Doh* and Hyoung Joon Choi†

Department of Physics and Center for Computational Studies of Advanced Electronic Material Properties, Yonsei University, Seoul 03722, Korea

(Dated: November 15, 2018)

Black phosphorus (BP), a layered van der Waals material, reportedly has a band gap sensitive to external perturbations and manifests a Dirac-semimetal phase when its band gap is closed. Previous studies were focused on effects of each perturbation, lacking a unified picture for the band-gap closing and the Dirac-semimetal phase. Here, using pseudospins from the glide-reflection symmetry, we study the electronic structures of mono- and bilayer BP and construct the phase diagram of the Dirac-semimetal phase in the parameter space related to pressure, strain, and electric field. We find that the Dirac-semimetal phase in BP layers is singly connected in the phase diagram, indicating the phase is topologically identical regardless of the gap-closing mechanism. Our findings can be generalized to the Dirac semimetal phase in anisotropic layered materials and can play a guiding role in search for a new class of topological materials and devices.

PACS numbers: 73.22.-f, 71.30.+h, 71.55.Ak, 73.21.-b

Two-dimensional (2D) materials have attracted much attention in applications and theories, since graphene was found to be easily producible through mechanical exfoliation. Graphene now becomes the typical example for the 2D Dirac semimetal with the linear band structure and high mobility. However, without a band gap, graphene has a limitation in applications for optical or switching devices. On the other hand, another group of 2D materials, such as transition-metal dichalcogenides, have intermediate band gaps and show applicability to electronic devices. Recently, black phosphorus (BP) [1], an allotrope of phosphorus, gains lots of attention as a new 2D layered system [2–4]. BP has a thickness-dependent band gap varying from 0.3 eV for the bulk [5–8] up to ~ 2 eV for the monolayer [6, 9–11], and it is remarkable with the emergence of the Dirac-semimetal phase [12–21] and the quantum Hall effect at low temperature [22].

BP has a layered puckered-honeycomb structure, as shown in Fig. 1 [23–25]. The interlayer interaction is mainly van der Waals interaction [26, 27], which makes the bulk sample easily cleaved to few-layered 2D samples. BP layers have strong in-plane anisotropy in the atomic structure, resulting in anisotropic electrical conduction [4, 7, 8, 28–30]. The band gap of BP is controllable by various external parameters such as pressure [5, 6, 8, 17, 18, 31], electric field [14, 16, 32, 33], and potassium doping [12, 13]. Very recently, BP is found to become a Dirac semimetal when its gap is closed [12–18], making a strong contrast with other 2D semiconducting materials. Electronic structures of BP have been studied successfully by tight-binding methods [6, 34, 35], density-functional methods [12–16, 18, 27, 28, 31, 32, 34, 35], and the GW method [34, 35]. However, a unified picture for the band-gap closing method and the Dirac-semimetal phase in BP layers is still lacking.

In this letter, we investigate key ingredients of BP to obtain a unified picture for the band-gap closing and the Dirac-semimetal phase. The gap-closing condition

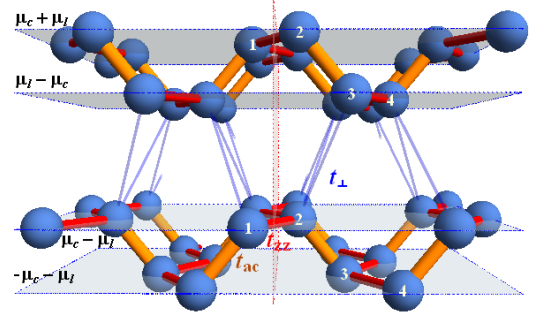


FIG. 1: (Color online) Atomic structure of bilayer BP. Red, orange, and blue bonds denote the intralayer hopping energy along the zigzag and armchair directions (t_{zz} and t_{ac}) and the interlayer hopping energy (t_{\perp}), respectively. The vertical red dotted plane denotes the glide-reflection symmetric plane. Each horizontal plane may have a different potential energy due to a vertical electric field. μ_c and μ_l are intra- and inter-layer potential difference, respectively. The number at each phosphorus atom is for the basis index in the unit cell.

is obtained in the parameter space of Hamiltonian that is related to pressure, strain, and external electric fields. From the glide-reflection (GR) symmetry of BP, pseudospins are derived, which guarantee a massless Dirac Hamiltonian when the band gap is closed. In each layer, the band gap can be closed by reducing the anisotropy of the intralayer hopping, while the interlayer coupling narrows the band gap in multilayer BP. We also find intra- and interlayer potential differences have opposite effects so that a perpendicular electric field does not decrease the band gap in the monolayer while it reduces the gap in the multilayer. Obtained phase diagrams show that the Dirac semimetal phase in BP layers is topologically identical regardless of the gap-closing method despite some difference in detailed electronic band structures.

Layered BP has four P atoms in the unit cell, as in-

dexed in Fig. 1. For a tight-binding model, one orbital per P atom can describe the electronic structure near the band gap [35]. Based on the tight-binding parameters extracted from the GW calculation [35], we construct a simple Hamiltonian which includes the nearest-neighbor intralayer hopping energies, $t_{zz} = -1.486$ eV and $t_{ac} = 3.729$ eV, along the zigzag and armchair directions, respectively, and the nearest-neighbor interlayer hopping energy $t_{\perp} = 0.524$ eV. Although we use these parameters to describe pristine BP systems, our major findings are valid independently of their detailed values. For the monolayer, the Hamiltonian in the momentum space is $H = \sum_{\mathbf{k}} \Psi_{\mathbf{k}}^{\dagger} \hat{H}_{\mathbf{k}} \Psi_{\mathbf{k}}$ with $\Psi_{\mathbf{k}}^{\dagger} = [e^{-ik_y d_1} c_{1,\mathbf{k}}^{\dagger}, c_{2,\mathbf{k}}^{\dagger}, e^{-ik_y d_1} c_{3,\mathbf{k}}^{\dagger}, c_{4,\mathbf{k}}^{\dagger}]$,

$$\hat{H}_{\mathbf{k}} = \begin{bmatrix} \mu_c & 2t_{zz}\cos\frac{k_x a}{2} & 0 & t_{ac}e^{ik_y b/2} \\ 2t_{zz}\cos\frac{k_x a}{2} & \mu_c & t_{ac}e^{-ik_y b/2} & 0 \\ 0 & t_{ac}e^{ik_y b/2} & -\mu_c & 2t_{zz}\cos\frac{k_x a}{2} \\ t_{ac}e^{-ik_y b/2} & 0 & 2t_{zz}\cos\frac{k_x a}{2} & -\mu_c \end{bmatrix}. \quad (1)$$

Here, $c_{i,\mathbf{k}}^{\dagger}$ ($c_{i,\mathbf{k}}$) is the electron creation (annihilation) operator of the orbital at the i th P atom in the unit cell with the momentum \mathbf{k} , and a and b are the unit-cell lengths along the zigzag (x) and armchair (y) directions, respectively. d_1 is the y -coordinate difference of the first and second atoms. We also introduce a puckering potential energy, μ_c , which can be controlled by an electric field perpendicular to the BP plane.

BP has a glide-reflection (GR) symmetry with respect to the plane at the middle of the zigzag chain as shown by the red dotted plane in Fig. 1. This symmetry exists regardless of the number of layers and even with perpendicular electric fields that generate nonzero intra- and interlayer potential differences. As the GR operator commutes with Hamiltonian, it is the Dirac-cone protecting nonsymmorphic symmetry [36] of gap-closed mono- and multilayer BP.

Using the GR symmetry, the Hamiltonian (S2) is block-diagonalized by a pseudospin representation [see Supplemental Material]:

$$\begin{aligned} \hat{H}_{\mathbf{k},1} &= (D + 2t_{zz}\cos\frac{k_x a}{2})\hat{\sigma}_x + t_{ac}\sin\frac{k_y b}{2}\hat{\sigma}_y, \\ \hat{H}_{\mathbf{k},2} &= (D - 2t_{zz}\cos\frac{k_x a}{2})\hat{\sigma}_x - t_{ac}\sin\frac{k_y b}{2}\hat{\sigma}_y, \end{aligned} \quad (2)$$

with $D = \sqrt{\mu_c^2 + t_{ac}^2 \cos^2(k_y b/2)}$. Here, $\hat{\sigma}_x$ and $\hat{\sigma}_y$ in $\hat{H}_{\mathbf{k},i}$ are Pauli matrices with respect to the pseudospins. Energy bands from $\hat{H}_{\mathbf{k},1}$ and $\hat{H}_{\mathbf{k},2}$ are $E_{\mathbf{k},1,\pm} = \pm\sqrt{\{D + 2t_{zz}\cos(k_x a/2)\}^2 + t_{ac}^2 \sin^2(k_y b/2)}$ and $E_{\mathbf{k},2,\pm} = \pm\sqrt{\{D - 2t_{zz}\cos(k_x a/2)\}^2 + t_{ac}^2 \sin^2(k_y b/2)}$, respectively. Because $D \geq 0$ and $t_{zz} < 0$, the energy gap is determined by $\hat{H}_{\mathbf{k},1}$.

Figure 2 shows our tight-binding band structures for different parameters. As seen in Fig. 2(a), pristine monolayer BP has a direct band gap at Γ in the Brillouin zone

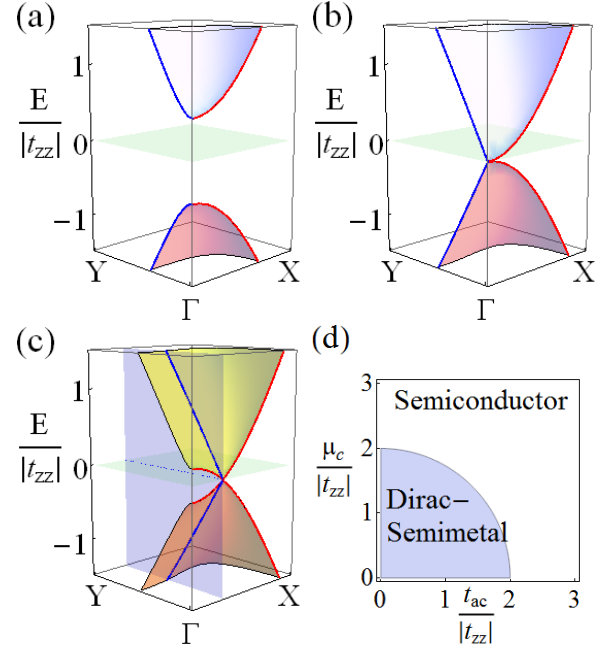


FIG. 2: (Color online) Tight-binding band structures near Γ in monolayer BP for (a) pristine, (b) $t_{ac}/|t_{zz}| = 2.0$, and (c) $t_{ac}/|t_{zz}| = 1.8$. (d) Phase diagram of monolayer BP. For overall band structures along high-symmetry lines, see Fig. S1 in Supplemental Material.

(BZ). Near Γ , the Hamiltonian $\hat{H}_{\mathbf{k},1}$ in (2) can be approximated as

$$\hat{H}_{\mathbf{k},1} \cong \left(\frac{1}{2}E_g + \frac{\hbar^2 k_x^2}{2m_x} + \frac{\hbar^2 k_y^2}{2m_y} - \frac{\hbar^2 v_y^2 k_y^2}{E_g} \right) \hat{\sigma}_x + \hbar v_y k_y \hat{\sigma}_y, \quad (3)$$

where the energy gap $E_g = 2\sqrt{\mu_c^2 + t_{ac}^2} + 4t_{zz}$, the zigzag effective mass $m_x = -2\hbar^2/(t_{zz}a^2)$, the armchair effective mass $m_y = -\hbar^2 E_g \sqrt{\mu_c^2 + t_{ac}^2}/(t_{zz}t_{ac}^2 b^2)$, and the armchair velocity $v_y = t_{ac}b/(2\hbar)$. The expression (3) is valid for positive or negative E_g . For zero E_g , all $k_y^2 \hat{\sigma}_x$ terms should be neglected together with E_g . The band dispersions in ΓY , that is, the armchair direction from Γ , are

$$E_{\mathbf{k},1,\pm} \simeq \pm \sqrt{E_g^2/4 + |t_{zz}|t_{ac}^2 b^2 k_y^2/(2\sqrt{\mu_c^2 + t_{ac}^2})}, \quad (4)$$

which are hyperbola whose asymptotic lines are $E = \pm \sqrt{t_{ac}^2 b^2 |t_{zz}|/(2\sqrt{\mu_c^2 + t_{ac}^2})} k_y$.

Monolayer BP is a honeycomb lattice in the sense that every P atom has three nearest neighbors. In the honeycomb lattice, an energy gap exists if the absolute values of the hopping energies to the three nearest neighbors cannot form a triangle [37–40]. In the case of pristine BP, $\mu_c = 0$ and there is a finite energy gap of $E_g = 1.514$ eV > 0 . This nonzero band gap is consistent with the triangular criterion, that is, monolayer BP is semiconducting because the hopping energy along the armchair direction is greater than twice the absolute

value of the hopping energy along the zigzag direction. If t_{ac} decreases or $|t_{zz}|$ increases, E_g will decrease. Thus, a way to modify the energy gap in BP layers is to apply pressure or strain which can change bond angles and bond lengths and thereby the intralayer hopping energies.

The above triangular criterion is modified when an external electric field is applied. We define a gap-closing parameter including the puckering potential energy μ_c ,

$$\beta_1 \equiv \left| \frac{t_{ac}}{2t_{zz}} \right| \sqrt{1 + \frac{\mu_c^2}{t_{ac}^2}}. \quad (5)$$

Then, monolayer BP has a finite energy gap when $\beta_1 > 1$, as in the case of the pristine monolayer [Fig. 2(a)], and the gap vanishes when $\beta_1 \leq 1$. At the moment of the gap closing ($\beta_1 = 1$), the Hamiltonian $\hat{H}_{\mathbf{k},1}$ becomes highly anisotropic Dirac Hamiltonian

$$\hat{H}_{\mathbf{k},1} \cong \frac{\hbar^2 k_x^2}{2m_x} \hat{\sigma}_x + \hbar v_y k_y \hat{\sigma}_y, \quad (6)$$

which results in a linear dispersion in the armchair direction (ΓY) and quadratic one in the zigzag direction (ΓX) [Fig. 2(b)]. This corresponds to the single merged Dirac point of the two separate Dirac points [41].

When $\beta_1 < 1$, monolayer BP is metallic, with the valence and conduction bands touching each other at finite momenta ($\pm k_D, 0$) in the ΓX line [Fig. 2(c)]. From the condition that $E_{\mathbf{k},1,+} = E_{\mathbf{k},1,-}$, we obtain

$$k_D = (2/a) \cos^{-1} \beta_1. \quad (7)$$

Near the crossing point, $(k_D, 0)$, the Hamiltonian $\hat{H}_{\mathbf{k},1}$ can be written as a massless Dirac particle,

$$\hat{H}_{\mathbf{k},1} \cong \hbar v_x (k_x - k_D) \hat{\sigma}_x + v_y k_y \hat{\sigma}_y, \quad (8)$$

where $v_x = -(t_{zz}a/\hbar) \sin(k_D a/2) = -(t_{zz}a/\hbar) \sqrt{1 - \beta_1^2}$. Thus, $(\pm k_D, 0)$ are Dirac points with anisotropic linear bands $E_{\pm}(\mathbf{k}) = \pm \hbar \sqrt{v_x^2 (k_x - k_D)^2 + v_y^2 k_y^2}$. Perpendicular electric field can generate μ_c , which re-opens the gap if it is large enough to make $\beta_1 > 1$. Now the phase diagram is constructed according to (5) in the parameter space of $(t_{ac}, \mu_c)/|t_{zz}|$ [Fig. 2(d)].

The pseudospin representations of the conduction- and valence-band states are $\frac{1}{\sqrt{2}}(1, e^{i\phi})$ and $\frac{1}{\sqrt{2}}(1, -e^{i\phi})$, respectively, when the Hamiltonian $\hat{H}_{\mathbf{k},1}$ in (2) is expressed as $\hat{H}_{\mathbf{k},1} = E_{\mathbf{k},1,+}(\cos \phi \hat{\sigma}_x + \sin \phi \hat{\sigma}_y)$. Then, the expectation value of the pseudospin vector, $\vec{\sigma}$, for a conduction-band state is $\langle \vec{\sigma} \rangle = \langle (\hat{\sigma}_x, \hat{\sigma}_y, \hat{\sigma}_z) \rangle = (\cos \phi, \sin \phi, 0)$, which lies in the xy -plane in our representation. Figure 3 shows the calculated $\langle \vec{\sigma} \rangle$ of the conduction and valence bands. We find that the y -component $\langle \hat{\sigma}_y \rangle$ of each band always changes the sign by the reflection across x -axis, that is

$$\langle \hat{\sigma}_y(k_x, k_y) \rangle = -\langle \hat{\sigma}_y(k_x, -k_y) \rangle \quad (9)$$

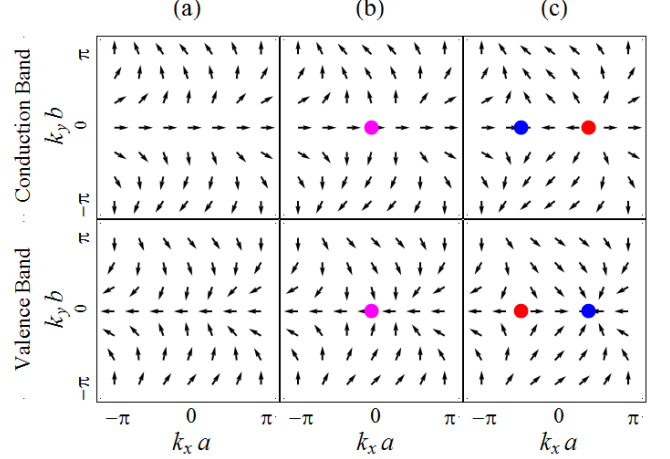


FIG. 3: (Color online) Pseudospin expectation values of conduction and valence bands in BZ for (a) the semiconducting, (b) the highly anisotropic Dirac semimetallic, and (c) the Dirac semimetallic phase. Colored dots in (b) and (c) are Dirac points.

in the semiconducting [Fig. 3(a)] as well as Dirac-semimetallic phases [Figs. 3(b) and (c)]. This sign-reversal reduces the back scattering of charge carriers moving along the armchair direction, enhancing their mobility even at the semiconducting phase, unless impurities or defects produce very abrupt potential. After the gap closing, the pseudospin becomes chiral around the Dirac points [Fig. 3(c)], enhancing the mobility in all directions.

BP has weak spin-orbit coupling (SOC) and the first-principles calculation showed that SOC takes place as $\hat{H}_{\text{SOC}} = \lambda_{\text{SOC}} \hat{S}_x \hat{\sigma}_y$ in the low-energy effective Hamiltonian [13], where λ_{SOC} is a constant and \hat{S}_x is the x -component of the real spin. Since this term does not break the GR symmetry, the Dirac point in semimetallic BP layers is still protected and only shifted in the k_y -direction. To open a band gap at the Dirac point, we need a mass term, which adds a $\hat{\sigma}_z$ term to (8). If the mass term is simply a constant times $\hat{\sigma}_z$, BP layers become a trivial insulator. However, if one can introduce, for example, a momentum-dependent mass term like

$$H_M = \lambda_M \sin(k_x a) \hat{\sigma}_z S_z, \quad (10)$$

it generates a topologically nontrivial energy gap at the Dirac point [42]. Realization and control of such perturbation in BP is of great interest because it will enable a topologically trivial-to-nontrivial phase transition.

Now we consider bilayer BP. We generalize the operator $c_{i,\mathbf{k}}$ to $c_{i,\mathbf{k},j}$, where $j = 1, 2$ indicates the first and second layer in the bilayer, and similarly $\Psi_{\mathbf{k}}$ to $\Psi_{\mathbf{k},j}$. Then, the Hamiltonian of the bilayer is

$$H = \sum_{\mathbf{k}} \left\{ \Psi_{\mathbf{k},1}^\dagger (\hat{H}_{\mathbf{k}} + \mu_l) \Psi_{\mathbf{k},1} + \Psi_{\mathbf{k},2}^\dagger (\hat{H}_{\mathbf{k}} - \mu_l) \Psi_{\mathbf{k},2} + \Psi_{\mathbf{k},1}^\dagger \hat{V}_{\mathbf{k}} \Psi_{\mathbf{k},2} + \Psi_{\mathbf{k},2}^\dagger \hat{V}_{\mathbf{k}}^\dagger \Psi_{\mathbf{k},1} \right\}, \quad (11)$$

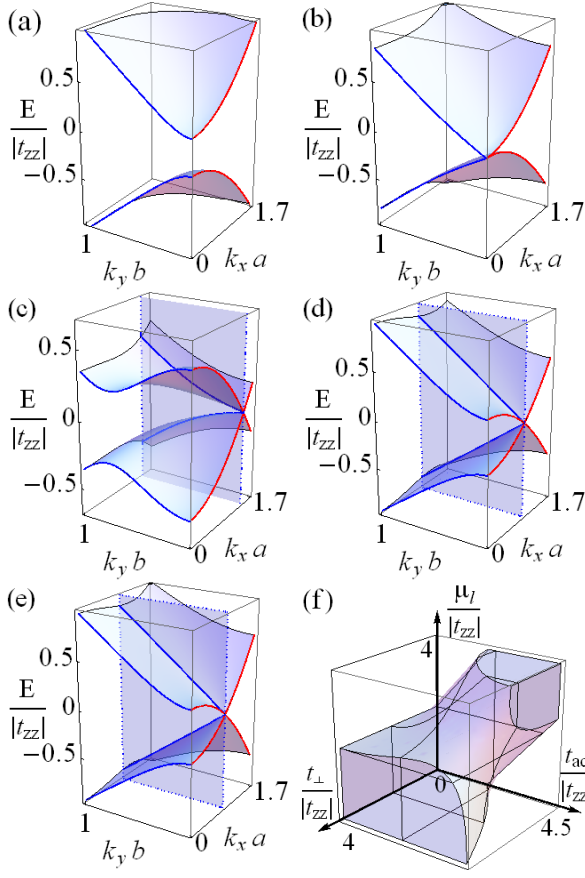


FIG. 4: (Color online) Tight-binding band structures near Γ in bilayer BP for (a) pristine, (b) $\mu_l/|t_{zz}| = 0.41$, (c) $\mu_l/|t_{zz}| = 1.0$, (d) $t_{ac}/|t_{zz}| = 2.05$, and (e) $t_{\perp}/|t_{zz}| = 0.95$. (f) Phase diagram of bilayer, where the dark region is the Dirac semimetal. For overall band structures along high-symmetry lines, see Fig. S2 in Supplemental Material.

where $\hat{H}_{\mathbf{k}}$ is the intralayer Hamiltonian (S2), μ_l is half of the difference in the average potentials of the two layers, and $\hat{V}_{\mathbf{k}}$ is due to the interlayer hopping. We assume that the first layer is placed on top of the second layer so that the third and fourth P atoms of the first layer are the nearest neighbors of the first and second P atoms of the second layer, as shown in Fig. 1. Then, $\hat{V}_{\mathbf{k}}$ is a 4×4 matrix $\begin{pmatrix} \hat{0} & \hat{0} \\ \hat{v}_{\mathbf{k}} & \hat{0} \end{pmatrix}$ with $\hat{v}_{\mathbf{k}} = 2t_{\perp} \cos \frac{k_x a}{2} (\cos \frac{k_y b}{2} \hat{\sigma}_x - \sin \frac{k_y b}{2} \hat{\sigma}_y)$ and $\hat{0}$ is 2×2 zero matrix.

Figures 4(a)-(e) show our tight-binding band structures of bilayer BP. Due to the GR symmetry of the lattice, the band-gap closing occurs at a point in the ΓX line in BZ [43]. For $k_y = 0$, one can exploit the GR symmetry and obtain the lowest conduction-band energy E_c and the highest valence-band energy E_v in the ΓX as

$$E_{c,v}(k_x) = \pm 2t_{zz} \cos(k_x a/2) \pm \sqrt{P_{k_x} - 2\sqrt{Q_{k_x}}} \quad (12)$$

where $+$ and $-$ are for conduction band and valence band, respectively, $P_{k_x} = 2t_{\perp}^2 \cos^2(k_x a/2) + t_{ac}^2 + \mu_l^2 + \mu_c^2$,

and $Q_{k_x} = t_{ac}^2 t_{\perp}^2 \cos^2(k_x a/2) + t_{ac}^2 \mu_l^2 + \{t_{\perp}^2 \cos^2(k_x a/2) - \mu_l \mu_c\}^2$. Then the Dirac point k_D is determined by the condition $E_c(k_D) = E_v(k_D)$. For the simplicity, we neglect μ_c , since μ_c has a smaller value than μ_l at an applied electric field. When $\mu_c = 0$, we define the gap-closing parameter β_2 of bilayer BP as

$$\beta_2 = \sqrt{\frac{2t_{zz}^2(t_{ac}^2 + \mu_l^2) - t_{\perp}^2 \mu_l^2 - \sqrt{F}}{8t_{zz}^2(t_{zz}^2 - t_{\perp}^2)}} \quad (13)$$

with $F = 4t_{zz}^2 t_{ac}^2 (t_{\perp}^2 t_{ac}^2 + 4t_{zz}^2 \mu_l^2 - 3t_{\perp}^2 \mu_l^2) + t_{\perp}^4 \mu_l^4$. When $\beta_2 > 1$, bilayer BP is semiconducting with a direct band gap at Γ . When $\beta_2 < 1$, bilayer BP is metallic with Dirac points at $(\pm k_D, 0)$ given by

$$k_D = (2/a) \cos^{-1} \beta_2. \quad (14)$$

In the case of pristine bilayer, $\beta_2 > 1$ so that it is semiconducting, as shown in Fig. 4(a). Here, due to the interlayer coupling t_{\perp} , the gap is smaller than in the monolayer.

The interlayer potential energy difference μ_l , which can be generated by applied electric field, decreases the energy gap of bilayer BP. As shown in Figs. 4(b) and (c), the increase of μ_l can close the band gap and induce the Dirac-semimetal phase. This is in contrast with the puckering potential energy μ_c that acts against the gap closing although μ_c is also generated by an electric field.

Figures 4(d) and (e) show the band-gap closing by reducing the armchair hopping and by increasing the interlayer hopping, respectively. Compared with these bands, the field-induced band structure in Fig. 4(c) displays non-monotonous dispersions of the conduction and valence bands in the ΓY line, where a minimum of their band-energy difference occurs away from Γ .

In bilayer BP, the interlayer coupling t_{\perp} decreases β_2 of (13), making the Dirac point appear more easily in bilayer than monolayer. Since the GR symmetry exists in multilayer BP, t_{\perp} does not mix different pseudospins of each layer, but it widens each band, resulting in a smaller band gap in a thicker BP layer. When the band gap is closed, the band dispersions from Γ to Y in Fig. 4(e) are monotonous similarly to the case of the armchair-hopping reduction [Fig. 4(d)], in contrast with the non-monotonous behavior in Fig. 4(c), as mentioned above. Applied pressure can contribute to the band-gap reduction and closing since it enhances the interlayer coupling by decreasing the interlayer distance.

From (13), we obtained the phase diagram of Dirac semimetal for bilayer BP in the three-dimensional parameter space of $(t_{ac}, \mu_l, t_{\perp})/|t_{zz}|$, as shown in Fig. 4(f). Here the parameters t_{ac} , μ_l , and t_{\perp} are changeable by strain, pressure, and electric fields, as discussed above. We find that the region for the Dirac semimetal phase is continuously connected [Fig. 4(f)], indicating that the Dirac-semimetal phase is topologically identical regardless of the gap-closing method.

In summary, we obtained a unified picture on the Dirac semimetal phase of BP layers. Phase diagrams are obtained for mono- and bilayer BP in the parameter space of the Hamiltonian. Phase-controlling parameters are identified to be (i) the anisotropy of the intralayer hopping, which can be changed by pressure or strain, (ii) the interlayer hopping, which can be enhanced by pressure, and (iii) the interlayer potential energy difference, which can be generated by electric fields. Pseudospins, originating from the glide-reflection symmetry of BP, exist even in the semiconducting phase and assure the Dirac-semimetal phase when the band gap is closed. The Dirac-semimetal phase in BP layers is singly connected in the parameter space, indicating it is of the same kind regardless of the gap-closing method. Our findings can be generalized to the Dirac-semimetal phase in anisotropic layered materials and can play a guiding role in search for a new class of topological materials and devices.

This work was supported by the NRF of Korea (Grant No. 2011-0018306).

* Email: clotho72@yonsei.ac.kr

† Email: h.j.choi@yonsei.ac.kr

- [1] P. W. Bridgman, *J. Am. Chem. Soc.* **36**, 1344 (1914).
- [2] L. Li, Y. Yu, G. J. Ye, Q. Ge, X. Ou, H. Wu, D. Feng, X. H. Chen, and Y. Zhang, *Nat. Nanotech.* **9**, 372 (2014).
- [3] F. Xia, H. Wang, and Y. Jia, *Nat. Commun.* **5**, 4458 (2014).
- [4] H. Liu, A. T. Neal, Z. Zhu, Z. Luo, X. Xu, D. Tománek, and P. D. Ye, *ACS Nano* **8**, 4033 (2014).
- [5] R. W. Keyes, *Phys. Rev.* **92**, 580 (1953).
- [6] Y. Takao, H. Asahina, and A. Morita, *J. Phys. Soc. Jpn* **50**, 3362 (1981).
- [7] Y. Akahama, S. Endo, and S.-i. Narita, *J. Phys. Soc. Jpn* **52**, 2148 (1983).
- [8] A. Morita, *Appl. Phys. A* **39**, 227 (1986).
- [9] L. Liang, J. Wang, W. Lin, B. G. Sumpter, V. Meunier, and M. Pan, *Nano Lett.* **14**, 6400 (2014).
- [10] V. Tran, R. Soklaski, Y. Liang, and L. Yang, *Phys. Rev. B* **89**, 235319 (2014).
- [11] L. Li, J. Kim, C. Jin, G. Ye, D. Y. Qiu, F. H. da Jornada, Z. Shi, L. Chen, Z. Zhang, F. Yang, K. Watanabe, T. Taniguchi, W. Ren, S. G. Louie, X. Chen, Y. Zhang, and F. Wang, *arXiv:1601.03103*.
- [12] J. Kim, S. S. Baik, S. H. Ryu, Y. Sohn, S. Park, B.-G. Park, J. Denlinger, Y. Yi, H. J. Choi, and K. S. Kim, *Science* **349**, 723 (2015).
- [13] S. S. Baik, K. S. Kim, Y. Yi, and H. J. Choi, *Nano Lett.* **15**, 7788 (2015).
- [14] Q. Liu, X. Zhang, L. B. Abdalla, A. Fazzio, and A. Zunger, *Nano Lett.* **15**, 1222 (2015).
- [15] R. Fei, V. Tran, and L. Yang, *Phys. Rev. B* **91**, 195319 (2015).
- [16] K. Dolui and S. Y. Quek, *Sci. Rep.* **5**, 11699 (2015).
- [17] Z. J. Xiang, G. J. Ye, C. Shang, B. Lei, N. Z. Wang, K. S. Yang, D. Y. Liu, F. B. Meng, X. G. Luo, L. J. Zou, Z. Sun, Y. Zhang, and X. H. Chen, *Phys. Rev. Lett.* **115**, 186403 (2015).
- [18] P.-L. Gong, D.-Y. Liu, K.-S. Yang, Z.-J. Xiang, X.-H. Chen, Z. Zeng, S.-Q. Shen, and L.-J. Zou, *Phys. Rev. B* **93**, 195434 (2016).
- [19] M. Ezawa, *New J. Phys.* **16**, 115004 (2014).
- [20] C. Dutreix, E. A. Stepanov, and M. I. Katsnelson, *Phys. Rev. B* **93**, 241404(R) (2016).
- [21] S. Yuan, E. van Veen, M. I. Katsnelson, and R. Roldán, *Phys. Rev. B* **93**, 245433 (2016).
- [22] L. Li, F. Yang, G. J. Ye, Z. Zhang, Z. Zhu, W. Lou, X. Zhou, L. Li, K. Watanabe, T. Taniguchi, K. Chang, Y. Wang, X. H. Chen, and Y. Zhang, *Nat. Nanotech. advance on* (2016).
- [23] R. Hultgren, N. S. Gingrich, and B. E. Warren, *J. Chem. Phys.* **3**, 351 (1935).
- [24] A. Brown and S. Rundqvist, *Acta Cryst.* **19**, 684 (1965).
- [25] L. Cartz, S. R. Srinivasa, R. J. Riedner, J. D. Jorgensen, and T. G. Worlton, *J. Chem. Phys.* **71**, 1718 (1979).
- [26] L. Pauling and M. Simonetta, *J. Chem. Phys.* **20**, 29 (1952).
- [27] S. Appalakondaiah, G. Vaitheeswaran, S. Lebègue, N. E. Christensen, and A. Svane, *Phys. Rev. B* **86**, 035105 (2012).
- [28] R. Fei and L. Yang, *Nano Lett.* **14**, 2884 (2014).
- [29] A. N. Rudenko, S. Brener, and M. I. Katsnelson, *Phys. Rev. Lett.* **116**, 246401 (2016).
- [30] T. Low, Y. Jiang, and F. Guinea, *Phys. Rev. B* **92**, 235447 (2015).
- [31] A. S. Rodin, A. Carvalho, and A. H. Castro Neto, *Phys. Rev. Lett.* **112**, 176801 (2014).
- [32] H. Guo, N. Lu, J. Dai, X. Wu, and X. C. Zeng, *J. Phys. Chem. C* **118**, 14051 (2014).
- [33] J. Dai and X. C. Zeng, *J. Phys. Chem. Lett.* **5**, 1289 (2014).
- [34] A. N. Rudenko and M. I. Katsnelson, *Phys. Rev. B* **89**, 201408 (2014).
- [35] A. N. Rudenko, S. Yuan, and M. I. Katsnelson, *Phys. Rev. B* **92**, 085419 (2015).
- [36] S. M. Young and C. L. Kane, *Phys. Rev. Lett.* **115**, 126803 (2015).
- [37] Y. Hasegawa, R. Konno, H. Nakano, and M. Kohmoto, *Phys. Rev. B* **74**, 033413 (2006).
- [38] V. M. Pereira, A. H. Castro Neto, and N. M. R. Peres, *Phys. Rev. B* **80**, 045401 (2009).
- [39] B. G. Kim and H. J. Choi, *Phys. Rev. B* **86**, 115435 (2012).
- [40] J.-M. Hou and W. Chen, *Sci. Rep.* **5**, 17571 (2015).
- [41] G. Montambaux, F. Piéchon, J.-N. Fuchs, and M. O. Goerbig, *Phys. Rev. B* **80**, 153412 (2009).
- [42] F. D. M. Haldane, *Phys. Rev. Lett.* **61**, 2015 (1988).
- [43] G. van Miert and C. M. Smith, *Phys. Rev. B* **93**, 035401 (2016).

Supplemental Material: Dirac-semimetal phase diagram of two-dimensional black phosphorus

Hyeonjin Doh* and Hyoung Joon Choi†
Department of Physics and Center for Computational Studies of Advanced
Electron Material Properties, Yonsei University, Seoul 03722, Korea
(Dated: November 15, 2018)

PACS numbers: 73.22.-f, 71.30.+h, 71.55.Ak, 73.21.-b

Derivation of Dirac Hamiltonian for monolayer black phosphorus

Our tight-binding Hamiltonian for the monolayer BP is expressed with local bases as

$$H = \sum_{\mathbf{R}} \left\{ t_{zz} (c_{1,\mathbf{R}}^\dagger c_{2,\mathbf{R}} + c_{1,\mathbf{R}}^\dagger c_{2,\mathbf{R}+a\hat{x}} + c_{3,\mathbf{R}}^\dagger c_{4,\mathbf{R}} + c_{3,\mathbf{R}}^\dagger c_{4,\mathbf{R}-a\hat{x}} + \text{h.c.}) \right. \\ \left. + t_{ac} (c_{2,\mathbf{R}}^\dagger c_{3,\mathbf{R}} + c_{1,\mathbf{R}+b\hat{y}}^\dagger c_{4,\mathbf{R}} + \text{h.c.}) \right. \\ \left. + \mu_c (c_{1,\mathbf{R}}^\dagger c_{1,\mathbf{R}} + c_{2,\mathbf{R}}^\dagger c_{2,\mathbf{R}} - c_{3,\mathbf{R}}^\dagger c_{3,\mathbf{R}} - c_{4,\mathbf{R}}^\dagger c_{4,\mathbf{R}}) \right\}. \quad (\text{S1})$$

Here, $c_{i,\mathbf{R}}^\dagger (c_{i,\mathbf{R}})$ is the electron creation (annihilation) operator of the orbital at the i th P atom in the unit cell at \mathbf{R} , and a and b are the unit-cell lengths along the zigzag and armchair directions, respectively. Here we set the x - and y -axis along zigzag and armchair direction, respectively. To obtain electric band structure, we define $c_{i,\mathbf{k}} = \frac{1}{\sqrt{N}} \sum_{\mathbf{R}} c_{i,\mathbf{R}} e^{i\mathbf{k} \cdot (\mathbf{R} + \mathbf{r}_i)}$, where \mathbf{r}_i is the position of the i th basis within the unit cell and N is the number of \mathbf{k} vectors. By Fourier transformation of $H = \sum_{\mathbf{k}} \Psi_{\mathbf{k}}^\dagger \hat{H}_{\mathbf{k}} \Psi_{\mathbf{k}}$ with $\Psi_{\mathbf{k}}^\dagger = [c_{1,\mathbf{k}}^\dagger e^{-ik_y d_1}, c_{2,\mathbf{k}}^\dagger, c_{3,\mathbf{k}}^\dagger e^{-ik_y d_1}, c_{4,\mathbf{k}}^\dagger]$, we obtain the momentum representation $\hat{H}_{\mathbf{k}}$ of (S1) as

$$\hat{H}_{\mathbf{k}} = \begin{bmatrix} \mu_c & 2t_{zz} \cos \frac{k_x a}{2} & 0 & t_{ac} e^{ik_y b/2} \\ 2t_{zz} \cos \frac{k_x a}{2} & \mu_c & t_{ac} e^{-ik_y b/2} & 0 \\ 0 & t_{ac} e^{ik_y b/2} & -\mu_c & 2t_{zz} \cos \frac{k_x a}{2} \\ t_{ac} e^{-ik_y b/2} & 0 & 2t_{zz} \cos \frac{k_x a}{2} & -\mu_c \end{bmatrix}, \quad (\text{S2})$$

which is Eq. (1) of the main text.

To find a necessary condition for a pseudospin basis, we suppose the low-energy effective Hamiltonian of (S2) can be written as a Dirac Hamiltonian with a linear dispersion in y -direction at $k_y = 0$. Then, it is written as

$$\hat{H}_{\mathbf{k}}^{eff} \simeq \dots + v_y k_y \hat{\sigma}_y + \dots, \quad (\text{S3})$$

in terms of a pseudospin basis. Here $\hat{\sigma}_y$ is the Pauli matrix whose basis represents a pseudospin in the BP system. If a symmetry operation preserves the Dirac Hamiltonian and transforms k_y to $-k_y$, the symmetry operation should transform the pseudospin S_y to $-S_y$. For monolayer BP, the glide-reflection (GR) operator T_{GR} , associated with the GR symmetry plane in Fig. 1 of the main text, can be written as

$$T_{GR} = e^{-ip_y \frac{d_1}{2}} e^{iX \frac{\pi}{2}} e^{ip_y \frac{d_1}{2}} e^{ip_x \frac{a}{2}}, \quad (\text{S4})$$

where X , p_x , and p_y operators are

$$X \equiv \sum_{\mathbf{k}\nu\nu'} \eta_{\nu\nu'} c_{\nu,(k_x,-k_y)}^\dagger c_{\nu',(k_x,k_y)}, \\ p_x \equiv \sum_{\mathbf{k}\nu} k_x c_{\nu,(k_x,k_y)}^\dagger c_{\nu,(k_x,k_y)}, \\ p_y \equiv \sum_{\mathbf{k}\nu} k_y c_{\nu,(k_x,k_y)}^\dagger c_{\nu,(k_x,k_y)},$$

respectively. Here $\eta_{\nu\nu'} = 1$ for $(\nu, \nu') = (1, 2), (2, 1), (3, 4),$ and $(4, 3)$, and it is zero otherwise. The Hamiltonian (S2) is symmetric under the glide-reflection operation and contains odd function of k_y in its matrix elements. Therefore, for the Hamiltonian to be written as a Dirac Hamiltonian in a pseudospin representation, the pseudospin operator should have the following symmetric property under the glide-reflection operator:

$$T_{GR} S_x T_{GR}^\dagger = S_x, \\ T_{GR} S_y T_{GR}^\dagger = -S_y. \quad (\text{S5})$$

Here, $S_i \equiv \sum_{\sigma\sigma'} \chi_{\sigma,\nu}^\dagger (\hat{\sigma}_i)_{\sigma\sigma'} \chi_{\sigma',\nu}$ is a pseudospin operator for $i = x, y, z$ and $\chi_{\sigma,\nu}$ is a pseudospinor for $\sigma = \uparrow, \downarrow$. Since we have four bases in a unit cell, we have two orthogonal pseudospins which are distinguished by the index $\nu = 1, 2$. These symmetry conditions correspond to the following symmetric operation on the pseudospinors:

$$T_{GR} \chi_{\sigma,\nu} T_{GR}^\dagger = e^{i\theta} \chi_{-\sigma,\nu}, \quad (\text{S6})$$

where the minus sign on σ means the opposite spin. The constant phase factor θ is independent of σ and ν .

Now we assume the pseudospin state can be written in terms of the basis function in the unit cell,

$$\chi_{\sigma,\nu} = a_{\sigma\nu,1} c_{1,\mathbf{k}} e^{ik_y d_1} + a_{\sigma\nu,2} c_{2,\mathbf{k}} \\ + a_{\sigma\nu,3} c_{3,\mathbf{k}} e^{ik_y d_1} + a_{\sigma\nu,4} c_{4,\mathbf{k}}. \quad (\text{S7})$$

The basis functions in the unit cell are transformed by the glide-reflection operator in the following way:

$$T_{GR} c_{1,(k_x,k_y)}^\dagger T_{GR}^\dagger = i e^{ik_x a/2} e^{ik_y d_1} c_{2,(k_x,-k_y)}^\dagger, \\ T_{GR} c_{2,(k_x,k_y)}^\dagger T_{GR}^\dagger = i e^{ik_x a/2} e^{-ik_y d_1} c_{1,(k_x,-k_y)}^\dagger, \\ T_{GR} c_{3,(k_x,k_y)}^\dagger T_{GR}^\dagger = i e^{ik_x a/2} e^{ik_y d_1} c_{4,(k_x,-k_y)}^\dagger, \\ T_{GR} c_{4,(k_x,k_y)}^\dagger T_{GR}^\dagger = i e^{ik_x a/2} e^{-ik_y d_1} c_{3,(k_x,-k_y)}^\dagger. \quad (\text{S8})$$

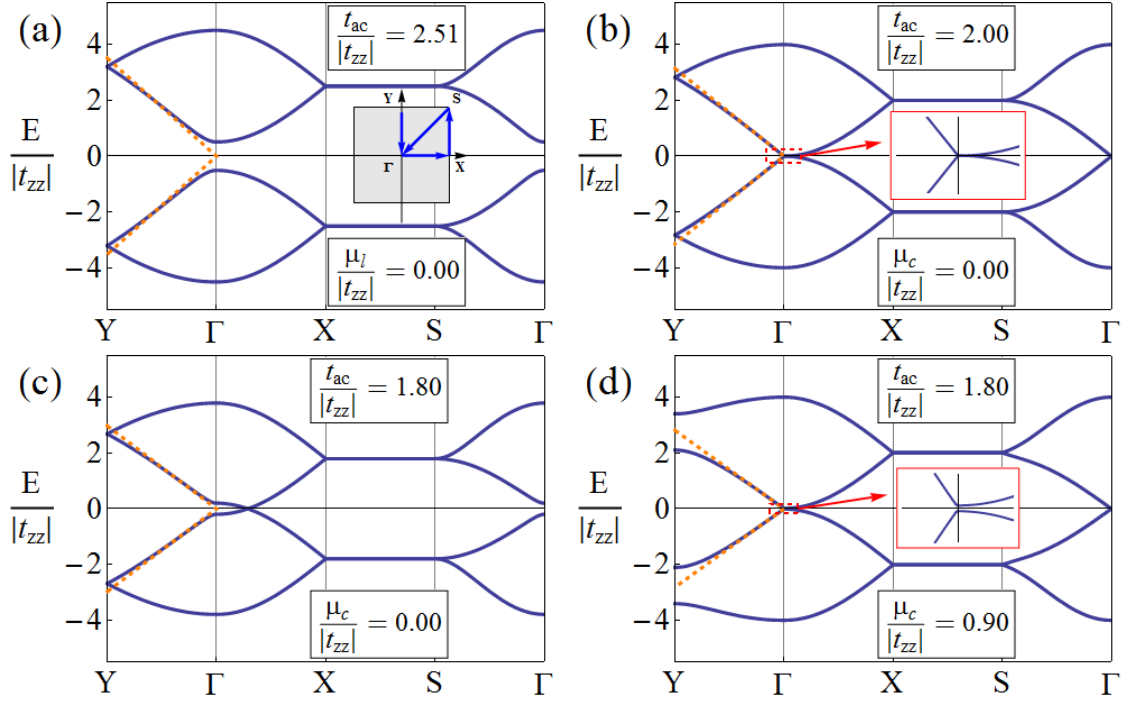


FIG. S5: Tight-binding band structures along high-symmetry lines in monolayer BP for (a) the pristine case, (b) t_{ac} reduced to $2|t_{zz}|$, (c) t_{ac} reduced to $1.8|t_{zz}|$, and (d) t_{ac} reduced to $1.8|t_{zz}|$ together with μ_c set to $0.9|t_{zz}|$. In (b)-(d), orange dashed lines are asymptotic lines. The inset in (a) shows the high-symmetry lines in the two-dimensional Brillouin zone. The insets in (b) and (d) enlarge band dispersions near Γ .

Using (S6), (S7), (S8), and an orthogonal condition $\chi_{\sigma,\nu}\chi_{\sigma',\nu'}^\dagger + \chi_{\sigma',\nu'}^\dagger\chi_{\sigma,\nu} = \delta_{\sigma\sigma'}\delta_{\nu\nu'}$, the pseudospin states can be written as

$$\begin{aligned} \chi_{\uparrow,1} &= \sin\theta_1 \sin\theta_2 c_{1,\mathbf{k}} e^{ik_y d_1} + \cos\theta_1 \cos\theta_2 c_{2,\mathbf{k}} \\ &\quad - \sin\theta_1 \cos\theta_2 c_{3,\mathbf{k}} e^{ik_y d_1} + \cos\theta_1 \sin\theta_2 c_{4,\mathbf{k}}, \\ \chi_{\downarrow,1} &= \cos\theta_1 \cos\theta_2 c_{1,\mathbf{k}} e^{ik_y d_1} + \sin\theta_1 \sin\theta_2 c_{2,\mathbf{k}} \\ &\quad + \cos\theta_1 \sin\theta_2 c_{3,\mathbf{k}} e^{ik_y d_1} - \sin\theta_1 \cos\theta_2 c_{4,\mathbf{k}}, \\ \chi_{\uparrow,2} &= \cos\theta_1 \sin\theta_2 c_{1,\mathbf{k}} e^{ik_y d_1} - \sin\theta_1 \cos\theta_2 c_{2,\mathbf{k}} \\ &\quad - \cos\theta_1 \cos\theta_2 c_{3,\mathbf{k}} e^{ik_y d_1} - \sin\theta_1 \sin\theta_2 c_{4,\mathbf{k}}, \\ \chi_{\downarrow,2} &= \sin\theta_1 \cos\theta_2 c_{1,\mathbf{k}} e^{ik_y d_1} - \cos\theta_1 \sin\theta_2 c_{2,\mathbf{k}} \\ &\quad + \sin\theta_1 \sin\theta_2 c_{3,\mathbf{k}} e^{ik_y d_1} + \cos\theta_1 \cos\theta_2 c_{4,\mathbf{k}}, \end{aligned} \quad (\text{S9})$$

where θ_1 and θ_2 are real numbers which are not determined yet. Now we block-diagonalize the Hamiltonian (S2) into two 2×2 matrices using the pseudospin states. We determine θ_1 and θ_2 to satisfy

$$\langle \chi_{\sigma,1} | \hat{H}_{\mathbf{k}} | \chi_{\sigma',2} \rangle = \langle \chi_{\sigma,2} | \hat{H}_{\mathbf{k}} | \chi_{\sigma',1} \rangle = 0 \quad (\text{S10})$$

for $\sigma = \uparrow, \downarrow$ and $\sigma' = \uparrow, \downarrow$. This condition yields

$$\begin{aligned} \tan(2\theta_1) &= \mu_c / (t_{ac} \cos(k_y b/2)), \\ \theta_2 &= \pi/4. \end{aligned} \quad (\text{S11})$$

Thus, the pseudospinors are related to the four atomic

orbitals in the unit cell as

$$\begin{aligned} \chi_{\uparrow,1} &= (\sin\theta_{\mathbf{k}} c_{1,\mathbf{k}} e^{ik_y d_1} + \cos\theta_{\mathbf{k}} c_{2,\mathbf{k}} \\ &\quad - \sin\theta_{\mathbf{k}} c_{3,\mathbf{k}} e^{ik_y d_1} + \cos\theta_{\mathbf{k}} c_{4,\mathbf{k}}) / \sqrt{2}, \\ \chi_{\downarrow,1} &= (\cos\theta_{\mathbf{k}} c_{1,\mathbf{k}} e^{ik_y d_1} + \sin\theta_{\mathbf{k}} c_{2,\mathbf{k}} \\ &\quad + \cos\theta_{\mathbf{k}} c_{3,\mathbf{k}} e^{ik_y d_1} - \sin\theta_{\mathbf{k}} c_{4,\mathbf{k}}) / \sqrt{2}, \\ \chi_{\uparrow,2} &= (\cos\theta_{\mathbf{k}} c_{1,\mathbf{k}} e^{ik_y d_1} - \sin\theta_{\mathbf{k}} c_{2,\mathbf{k}} \\ &\quad - \cos\theta_{\mathbf{k}} c_{3,\mathbf{k}} e^{ik_y d_1} - \sin\theta_{\mathbf{k}} c_{4,\mathbf{k}}) / \sqrt{2}, \\ \chi_{\downarrow,2} &= (\sin\theta_{\mathbf{k}} c_{1,\mathbf{k}} e^{ik_y d_1} - \cos\theta_{\mathbf{k}} c_{2,\mathbf{k}} \\ &\quad + \sin\theta_{\mathbf{k}} c_{3,\mathbf{k}} e^{ik_y d_1} + \cos\theta_{\mathbf{k}} c_{4,\mathbf{k}}) / \sqrt{2} \end{aligned} \quad (\text{S12})$$

with $\sin(2\theta_{\mathbf{k}}) = \mu_c/D$, $\cos(2\theta_{\mathbf{k}}) = (t_{ac}/D) \cos(k_y b/2)$, and $D = \sqrt{\mu_c^2 + t_{ac}^2 \cos^2(k_y b/2)}$. We define pseudospinor vector $\hat{X}_{\mathbf{k}} = [\chi_{\uparrow,1,\mathbf{k}}, \chi_{\downarrow,1,\mathbf{k}}, \chi_{\uparrow,2,\mathbf{k}}, \chi_{\downarrow,2,\mathbf{k}}]$. Then its relation to $\hat{\Psi}_{\mathbf{k}}$ can be expressed as

$$\hat{X}_{\mathbf{k}} = \hat{U}_{\mathbf{k}} \hat{\Psi}_{\mathbf{k}}, \quad (\text{S13})$$

using a unitary matrix

$$\hat{U}_{\mathbf{k}} = \frac{1}{\sqrt{2}} \begin{bmatrix} \sin\theta_{\mathbf{k}} & \cos\theta_{\mathbf{k}} & -\sin\theta_{\mathbf{k}} & \cos\theta_{\mathbf{k}} \\ \cos\theta_{\mathbf{k}} & \sin\theta_{\mathbf{k}} & \cos\theta_{\mathbf{k}} & -\sin\theta_{\mathbf{k}} \\ \cos\theta_{\mathbf{k}} & -\sin\theta_{\mathbf{k}} & -\cos\theta_{\mathbf{k}} & -\sin\theta_{\mathbf{k}} \\ \sin\theta_{\mathbf{k}} & -\cos\theta_{\mathbf{k}} & \sin\theta_{\mathbf{k}} & \cos\theta_{\mathbf{k}} \end{bmatrix} \quad (\text{S14})$$

These pseudospin bases block-diagonalize the Hamilto-

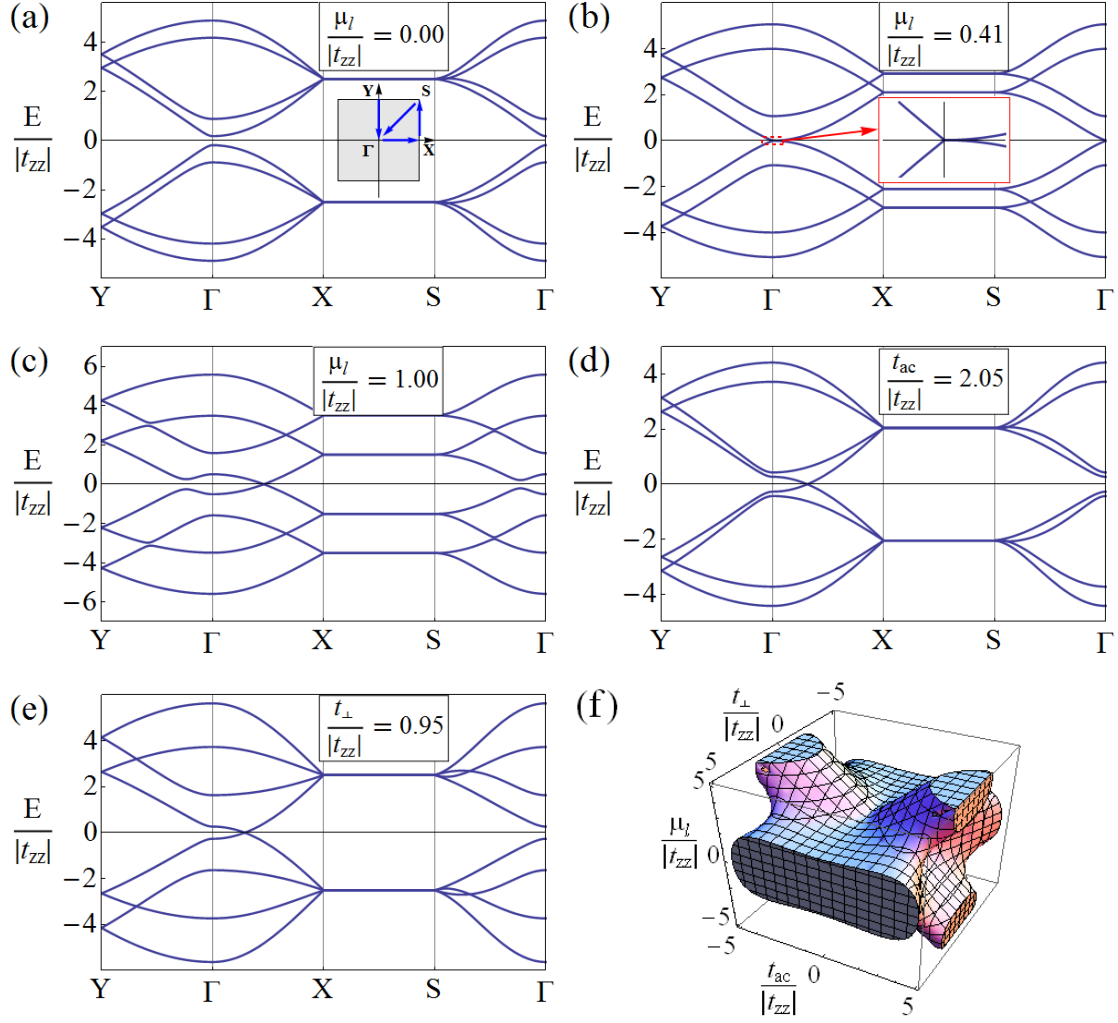


FIG. S6: Tight-binding band structures along high-symmetry lines in bilayer BP for (a) the pristine case, (b) μ_l set to $0.41|t_{zz}|$, (c) μ_l set to $|t_{zz}|$, (d) t_{ac} reduced to $2.05|t_{zz}|$, and (e) t_{\perp} increased to $0.95|t_{zz}|$. The inset in (a) shows the high-symmetry lines in the two-dimensional Brillouin zone. The inset in (b) enlarges the band dispersions near Γ . (f) Region of the Dirac-semimetal phase in the parameter space of $(t_{ac}, \mu_l, t_{\perp})/|t_{zz}|$. In (f), the parameter space is larger than that in Fig. 4(f) in the main text which covers $t_{ac} \geq 0$, $\mu_l \geq 0$, and $t_{\perp} \geq 0$ only.

nian (S2) to two 2×2 blocks:

$$\hat{U}_{\mathbf{k}} \hat{H}_{\mathbf{k}} \hat{U}_{\mathbf{k}}^{\dagger} = \begin{bmatrix} 0 & f_{\mathbf{k}}^{+} - i g_{\mathbf{k}} & 0 & 0 \\ f_{\mathbf{k}}^{+} + i g_{\mathbf{k}} & 0 & 0 & 0 \\ 0 & 0 & 0 & f_{\mathbf{k}}^{-} + i g_{\mathbf{k}} \\ 0 & 0 & f_{\mathbf{k}}^{-} - i g_{\mathbf{k}} & 0 \end{bmatrix} \quad (\text{S15})$$

with

$$f_{\mathbf{k}}^{\pm} = \sqrt{\mu_c^2 + t_{ac}^2 \cos^2(k_y b/2)} \pm 2t_{zz} \cos(k_x a/2),$$

$$g_{\mathbf{k}} = t_{ac} \sin(k_y b/2).$$

Now we have two Dirac-type Hamiltonians

$$\begin{aligned} \hat{H}_{\mathbf{k},1} &= f_{\mathbf{k}}^{+} \hat{\sigma}_x + g_{\mathbf{k}} \hat{\sigma}_y, \\ \hat{H}_{\mathbf{k},2} &= f_{\mathbf{k}}^{-} \hat{\sigma}_x - g_{\mathbf{k}} \hat{\sigma}_y, \end{aligned} \quad (\text{S16})$$

which correspond to Eq. (2) of the main text. These Dirac-type Hamiltonians are valid in the semiconducting phase as well as the Dirac-semimetal phase.

Tight-binding band structures along high-symmetry lines

Figures S1 and S2 show overall electronic band structures along high-symmetry lines in mono- and bilayer black phosphorus (BP) obtained from our tight-binding model described in the main text. Figures S1 and S2 correspond to Figs. 2 and 4 in the main text, respectively.